RSC Advances

PAPER

View Article Online
View Journal | View Issue

Cite this: *RSC Adv.*, 2025, **15**, 11327

Efficient Rhodamine B degradation *via* Fenton-like and E-Fenton processes using magnetic biochar from rubber seed shells

My Linh Nguyen,[a] Thanh Tung Nguyen[b] and Hoang Long Ngo *[b]

This study evaluates the potential of magnetic biochar derived from rubber seed shells for the Rhodamine B (RhB) removal using Fenton-like and electro-Fenton (E-Fenton) processes. The magnetic catalyst was synthesized by pyrolyzing rubber seed shell and incorporating α-FeOOH *via* precipitation. Characterization techniques, including XRD, SEM, EDX, and FTIR, confirmed successful integration of iron into the biochar matrix, enhancing its catalytic efficiency. Under optimized conditions (pH 3, catalyst dosage of 0.5 g L^{-1}, H_2O_2 concentration of 20 mM, initial RhB concentration of 100 mg L^{-1}, current of 150 mA, electrode distance of 2 cm, and contact time of 120 minutes), the ideal magnetic biochar (RBCF12) exhibited a RhB degradation efficiency of 91.67%. Kinetic studies revealed that the degradation followed a pseudo-first-order model. The degradation efficiency of RBCF12 remained over 60% after 6 consecutive runs, demonstrating its high stability and reusability for practical wastewater treatment applications. This research highlights the efficiency of magnetic biochar as a cost-effective, sustainable material for advanced oxidation processes. Additionally, by leveraging both Fenton-like and E-Fenton processes, it offers a robust and eco-friendly solution to address dye contamination in industrial effluents, contributing to the development of more sustainable and efficient wastewater treatment practices.

Received 21st February 2025
Accepted 31st March 2025

DOI: 10.1039/d5ra01265a

rsc.li/rsc-advances

Introduction

The textile and garment industry is a cornerstone of Vietnam's economy, with export turnover reaching $44 billion in 2022, a 10% increase compared to 2021, making Vietnam one of the top three global textile exporters with a market share of 4–5%.[1,2] However, approximately 15 to 20% of dye residues are directly released in the environment during the dyeing process.[3] As the European Union enforces new sustainability strategies, including requirements for recycling, reusability, and extended product lifespans, the industry faces increasing demands to adopt greener production methods.[4,5] A critical aspect of this transition is addressing wastewater generated by textile processes, which contain diverse pollutants, particularly dyes such as Rhodamine B (RhB).[6,7] RhB is widely used in textile manufacturing, with a concentration in textile effluents of about 150–3000 mg L^{-1}.[8] It poses significant environmental and health risks, including water pollution, ecological toxicity, and carcinogenic effects.[9,10] As a result, removal of RhB from textile wastewater is of the utmost importance.

Current wastewater treatment methods, including biological degradation, adsorption, and flocculation, are often inadequate as they transform pollutants to sludge and thus generate secondary waste. Besides, these techniques might be inefficient, complex, energy-consuming, difficult to operate, and expensive to be applied in the practical.[11,12] These limitations require the development of more innovative and efficient methods for the treatment of wastewater. Heterogeneous Fenton processes have recently emerged as one of the most effective methods for dye degradation, utilizing solid iron-based catalysts and hydrogen peroxide (H_2O_2) to generate highly reactive hydroxyl radicals ($^{\bullet}OH$) (eqn (1)), which break down organic pollutants.[13,14] However, H_2O_2 depletion and slow Fe^{2+} regeneration (eqn (2)) significantly limit the continuous $^{\bullet}OH$ generation in this conventional Fenton process. To solve this problem, the electro-Fenton (e-Fenton) was developed, which employs the electrocatalytic oxygen reduction reaction (ORR) to H_2O_2 (eqn (3)) followed by the transformation of the newly generated H_2O_2 to $^{\bullet}OH$ by Fe^{2+}, therefore continuously generating $^{\bullet}OH$.[15] More importantly, Fe^{2+} can also be regenerated continuously at the cathode, thus enabling the continuous generation of $^{\bullet}OH$ (eqn (4)). As a result, the E-Fenton process not only accelerates the organic pollutant degradation but also reduces sludge formation and extends the pH range for effective operation.[16,17]

$$Fe^{2+} + H_2O_2 \rightarrow Fe^{3+} + OH^- + {}^{\bullet}OH \quad (1)$$

[a]*Department of Environmental Technology, Faculty of Chemical and Food Technology, HCMC University of Technology and Education, 1 Vo Van Ngan Street, Linh Chieu Ward, Thu Duc City, Ho Chi Minh City, Vietnam. E-mail: longnh@ntt.edu.vn*

[b]*NTT Hi-Tech Institute, Nguyen Tat Thanh University, 300A Nguyen Tat Thanh Street, Ward 13, District 4, Ho Chi Minh City, Vietnam*

$$Fe^{3+} + H_2O_2 \rightarrow Fe^{2+} + HO_2^{\cdot} + H^+ \quad (2)$$

$$O_2 + 2H^+ + 2e^- \rightarrow H_2O_2 \quad (3)$$

$$Fe^{3+} + e^- \rightarrow Fe^{2+} \quad (4)$$

As previously mentioned, the e-Fenton process is significantly influenced by the rate of H_2O_2 formation.[18,19] In this manner, noble-metal-based catalysts have exhibited outstanding ORR catalytic activity and high H_2O_2 selectivity, but their high cost and limited availability have made it difficult to use them in wastewater treatment.[20,21] Recently, carbon materials have attracted a lot of interest in the H_2O_2 producing process thanks to their high potential for hydrogen evolution, low catalytic activity in H_2O_2 decomposition, high conductivity and stability, as well as their abundance, environmental friendliness, low cost and easy fabrication.[22,23] Among them, biochar, which is derived from renewable biomass such as agricultural residues, serves as an economical and eco-friendly substrate for Fenton catalysts due to its high porosity and abundance of surface functional groups.[24,25]

Among the abundant agricultural residues in Vietnam, rubber seed shells offer a renewable and cost-effective biomass source for the synthesis of biochar and activated carbon. Their high porosity and surface functional groups make them an ideal substrate for iron oxide modification, enabling efficient catalytic activity in the Fenton-like and E-Fenton processes. In this study, rubber seed shells were employed to synthesize biochar modified with iron oxides. This material was employed as a heterogeneous catalyst in the Fenton-like and E-Fenton processes for the degradation of RhB. The study investigates the effects of different operational parameters, such as pH, catalyst dosage, and H_2O_2 concentration on the RhB degradation efficiency. Kinetic and thermodynamic analyses were also performed to provide insights into the degradation mechanism, presenting an efficient and sustainable approach for textile wastewater treatment.

Experimental section

Materials and chemicals

Rubber seed shells were sourced from rubber plantations in Ben Cat City, Binh Duong Province, Vietnam. Rhodamine B ($C_{28}H_{31}ClN_2O_3$, ≥95%) was obtained from Amresco, China. Iron(III) nitrate nonahydrate ($Fe(NO_3)_3 \cdot 9H_2O$) was provided by Sigma-Aldrich. Hydrogen peroxide (H_2O_2, 30%), H_2SO_4 and NaOH was purchased from Chemsol Chemical Company, Vietnam. Deionized water was employed during all of the experimental procedures. All reagents were used as supplied.

Fabrication and characterization of magnetic biochar derived from rubber seed shells

Rubber seed shells were collected, thoroughly washed, and dried. The dried shells were then pulverized and subjected to anaerobic pyrolysis at 500 °C for 2 hours. After cooling to room temperature, the resulting rubber-seed-shell biochar (RBC) was sieved through a 0.2 mm mesh. Iron-oxide-loaded biochar catalyst (RBCF) was prepared *via* co-precipitation method using $Fe(NO_3)_3 \cdot 9H_2O$ as the iron precursor. Initially, 5 g of RBC was dispersed in 200 mL of deionized water and the mixture was stirred vigorously for 30 minutes. Subsequently, 10 g of $Fe(NO_3)_3 \cdot 9H_2O$ was added, which was then stirred continuously for 2 hours. To regulate the pH and avoid the formation of $Fe(OH)_3$, 1.0 M NaOH solution was added dropwise until pH 12. The mixture was then heated at 60 °C for 12 hours to facilitate the iron deposition on the biochar. After the reaction, the RBCF material was thoroughly rinsed three to four times with deionized water until pH 7. Finally, the material was dried at 60 °C for 24 hours. The preparation process and parameters, adapted from previous studies,[26–28] ensured optimal conditions for preparing the magnetic biochar catalyst with enhanced catalytic properties. The names of corresponding RBCF materials are summarized in Table 1.

Table 1 RBCF materials and their corresponding composition

RBCF materials	RBC/$Fe(NO_3)_3 \cdot 9H_2O$ ratio	RBC (g)	$Fe(NO_3)_3 \cdot 9H_2O$ (g)
RBC	—	5	—
RBCF21	2 : 1	10	5
RBCF11	1 : 1	5	5
RBCF12	1 : 2	5	10

The structure and morphology of the RBCF catalysts were examined using Bruker D6 Advance X-ray Diffractometer (XRD) with Cu Kα irradiation (40 kV, 40 mA) from 10 to 70°, and Hitachi S-4800 field emission scanning electron microscope (FESEM) equipped with X-ray energy dispersive spectroscopy (EDS). Surface properties of the catalysts were investigated using Agilent Cary 630 Fourier transform infrared spectrometer (FTIR) in the range of 650–4000 cm^{-1}.

Degradation of Rhodamine B

The degradation of Rhodamine B (RhB) was studied using either batch Electro-Fenton or heterogeneous Fenton process to optimize operational parameters for maximum RhB removal efficiency. The experiment was set up as described in our previous publication, including a 600 mL cylindrical glass reactor equipped with a TES 6102 DC power supply, a dimensionally stable anode (DSA) connected to positive terminal, and a titanium cathode (8 cm × 3 cm) connected to the negative terminal.[29] The electrodes, spaced 2 cm apart, allowed for adjustable current from 0 to 5 A, were monitored using an ammeter. The catalyst and 100 mL of 100 mg per L RhB solution were mixed and agitated with a magnetic stirrer to ensure homogeneity during the reaction.

Both Electro-Fenton and heterogeneous Fenton processes were investigated by systematically varying parameters, including pH from 2 to 9, catalyst dose from 0.5 to 2.5 g L^{-1}, hydrogen peroxide concentration from 10 to 30 mM, and initial RhB concentration from 50 to 1000 mg L^{-1}. For the e-Fenton process, electrode distance and electric current were additionally varied from 1 to 4 cm and from 50 to 200 mA, respectively. The reaction mixture was shaken at 200 rpm for

a predetermined time under specific conditions. Following the reaction, the mixture was filtered through a 0.45 μm microfiltration membrane to separate solids from the liquid phase before analysis.

The RhB concentration in the filtrate was analyzed using a Hitachi U-2910 UV-Vis Double-Beam Spectrophotometer at 552 nm (maximum absorption wavelength). The final RhB concentrations were calculated from the standard curve equation based on the correlation between RhB concentration and optical absorbance. The RhB removal efficiency (H%) was calculated by eqn (5). Control experiments were performed without the catalyst to establish a baseline for comparison. To evaluate the post-reaction properties of the catalyst, solids retained on the filter paper were dried at 105 °C for 24 hours before further analysis. All of the experiments were conducted three times. After triplicated experiments, the standard deviations were calculated and used for error bars.

$$H\% = \left(1 - \frac{C_t}{C_0}\right) \times 100 \quad (5)$$

with H% being the RhB removal efficiency (%), C_0 being the initial RhB concentration (mg L^{-1}), and C_t being the RhB concentration (mg L^{-1}).

Degradation kinetics and mechanism

The degradation rate constant was calculated using the values obtained by fitting the linear part of the kinetic curve in the first 30 minutes to the pseudo-first-order kinetic model with a high correlation coefficient (R^2), as shown in eqn (6).[30]

$$C_t = C_0 e^{-kt} \quad (6)$$

with C_t being the RhB concentration, C_0 being the initial RhB concentration, k being the initial degradation rate constant, and t being the time.

Results and discussion

Characterizations of catalysts

As observed in the FTIR spectra of three iron-oxide-loaded biochar (Fig. 1a), all of the RBCF samples exhibit the absorption bands of biochar. Specifically, the absorption bands at around 3455 cm^{-1} and 1400 cm^{-1} can be attributed to the –OH stretching vibration and C–O–H deformation vibration, respectively, which belong to abundant oxygen-containing functional groups on the biochar surface.[31] Meanwhile, the absorption peak at 1560 cm^{-1} can be accredited to the aromatic C–C stretching vibration, which was due to the high carbon content of the biochar.[31,32] In addition, the appearance of the α-FeOOH phase was confirmed by the absorption bands from 900 cm^{-1} to 600 cm^{-1}, which was assigned to the Fe–O and Fe–OH bending vibrations. Particularly, the characteristic bands of Fe–O–OH bending vibration in α-FeOOH can be observed at 840 cm^{-1} and 910 cm^{-1}, whereas Fe–O stretching vibrations of goethite lattice can be recognized at 674 cm^{-1} and 431 cm^{-1},[33,34] and the Fe–O stretching vibration of Fe_3O_4 can be found at 585 cm^{-1}.[35]

In the XRD diagrams (Fig. 1b), the (002) plane of amorphous carbon from biomass-derived biochar can be observed at the broad peak of 21.56°.[36,37] Besides, the (110), (130), (111), (140) and (221) characteristic planes of α-FeOOH can be found at 2θ of 34.02, 35.38, 37.46, 54.57, and 63.94°, respectively.[38–40]

In the SEM image of RBC samples (Fig. 2a), the smooth and large surface of carbon can be observed.[41] In the RBCF12 sample, iron particles are found to be densely attached to the carbon surface (Fig. 2c),[42,43] confirming the successful preparation of RBCF materials. After the e-Fenton process (Fig. 2d), there was a decrease in the density of iron on the RBCF12 surface, as the iron particles participated in the Fenton process and may be leached from the materials.[42,43]

As presented in Table 2, the EDX results verify the presence of C, O, Na and Fe in the RBCF12 before the e-Fenton process. Fe was successfully doped onto the RBC material, making up around 4% of the mass of the RBCF12 material, whereas C and O were present in the original RBC and Na was from NaOH present during the preparation process. The iron content dropped following the e-Fenton process, indicating that Fe^{3+} was leaching from the RBCF12 catalyst.

Effect of pH. pH is one of the parameters that strongly influence the Fenton processes, not only the degradation efficiency but also the degradation rate. As observed in Fig. 3a, after 120 minutes at pH 2, the Fenton-like efficiencies of RBCF21, RBCF11, and RBCF12 were 64.0, 74.0, and 88.0%, respectively,

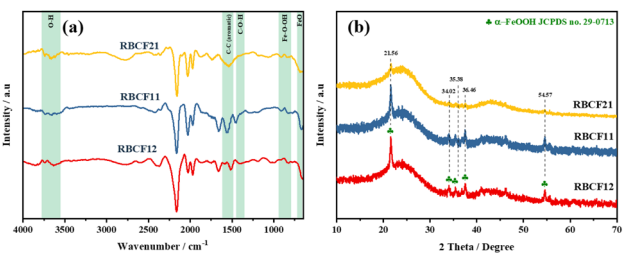

Fig. 1 (a) FT-IR spectra and (b) XRD pattern of RBCF samples before and after Fenton process.

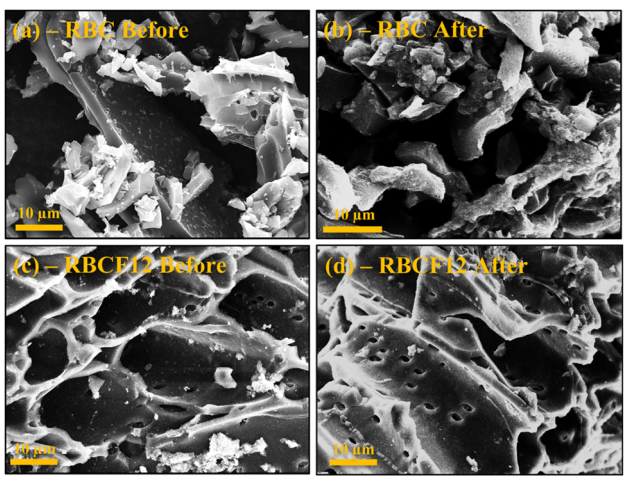

Fig. 2 SEM images of RBC (a) before and (b) after Fenton process; and RBCF12 (c) before and (d) after e-Fenton process.

Table 2 RBCF12 materials and their corresponding composition during the e-Fenton test

	Mass%	
Element	Before e-Fenton process	After e-Fenton process
C	88.52 ± 1.42	89.36 ± 1.15
O	6.12 ± 1.00	10.42 ± 1.08
Na	0.15 ± 0.14	ND
Si	0.43 ± 0.23	0.22 ± 0.14
Fe	4.78 ± 2.89	ND

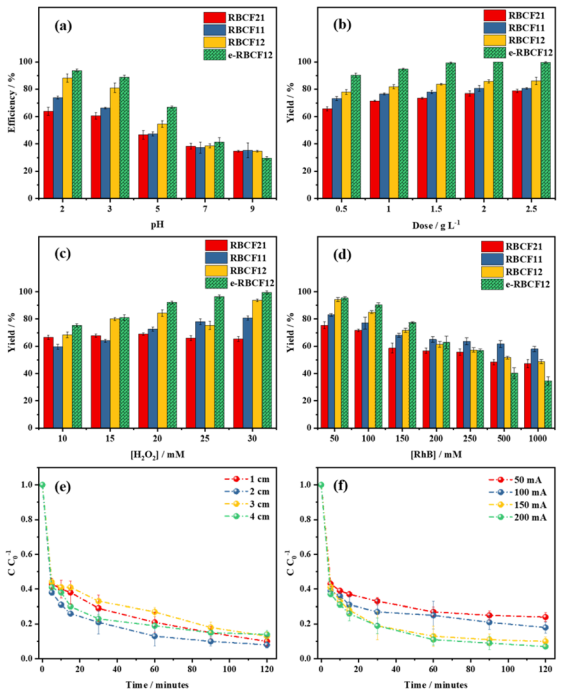

Fig. 3 The effect of different parameters on the Fenton-like and electro-Fenton degradation of RhB: (a) pH of 2–9 (C_0 = 100 mg L^{-1}, dose = 0.5 g L^{-1}, time = 120 min, H_2O_2 = 20 mM) (b) catalyst dose of 0.25–2.5 g L^{-1} (C_0 = 100 mg L^{-1}, pH = 3, time = 120 min, H_2O_2 = 20 mM) (c) H_2O_2 of 10–30 mM (C_0 = 100 mg L^{-1}, pH = 3, dose = 0.5 g L^{-1}, time = 120 min) (d) RhB initial concentration C_0 of 50–1000 g mL^{-1} (pH = 3, dose = 0.5 g L^{-1}, time = 120 min, H_2O_2 = 20 mM) (e) electrode distance of 1–4 cm (C_0 = 100 mg L^{-1}, pH = 3, dose = 0.5 g L^{-1}, H_2O_2 = 20 mM, electric current = 150 mA, time = 120 min) (f) electric current of 50–200 mA (C_0 = 100 mg L^{-1}, pH = 3, dose = 0.5 g L^{-1}, H_2O_2 = 20 mM, electrode distance = 2 cm, time = 120 min).Factors influencing Fenton-like process for Rhodamine B degradation

which was slightly increased to 93.7% in the electrochemical Fenton process. At pH 3, these values decreased to 60.7, 66.3, 81.0 and 88.7%, respectively. At higher pH such as 5, 7 or 9, the RhB degradation efficiency decreased gradually, to approximately 30–60%. It can be explained that, as pH increases to above 4, the degradation efficiency decreases owing to the precipitation of iron hydroxide as well as the reduction of the oxidation potential of $^{\bullet}OH$ radicals.[44] Therefore, it is concluded that the experiment should not be carried out at elevated pH (>3.0).[31] Additionally, in this study, although the highest Fenton-like and e-Fenton efficiency values of RBCF12 were achieved at pH 2, it was not significantly better than at pH 3, but more chemicals were utilized for pH adjustment. For this reason, pH 3 was selected as the optimized pH condition in the following experiments, which was similar to other previous publications.[26,39,45]

Effect of catalyst dose. As presented in Fig. 3b, increasing the RBCF catalyst amount from 0.5 to 2.5 g L^{-1} did not have a clear effect on the Fenton-like or e-Fenton degradation of RhB. Specifically, when the catalyst dose increased from 0.5 to 2.0 g L^{-1}, the degradation efficiency gradually increased from 65.7, 73.3, 78.0 and 90.3% to 78.7, 80.7, 86.0 and 100.2% for RBCF21, RBCF11, RBCF12, and e-RBCF12, respectively. However, as the catalyst amount reached 2.5 g L^{-1}, the degradation efficiency decreased slightly, to 78.7, 80.7, 86.0 and 99.7%, respectively. It can be explained that the increase of iron concentration present in RBCF catalysts could accelerate the H_2O_2 decomposition and increase the $^{\bullet}OH$ radical production. Moreover, the RhB amount that can be adsorbed on the catalyst surface also increased as the catalyst amount increased. This phenomenon can be elucidated using the homogeneous Fenton mechanism,[46,47] and will be discussed in detail in the proposed degradation mechanism section afterwards. When the catalyst dose increases, the degradation efficiency will increase thanks to the increase in the $^{\bullet}OH$ radical concentration in the solution (eqn (7)–(9)).[48] However, if the catalyst dose is too high, the degradation efficiency will drop as the excess catalyst will use up the $^{\bullet}OH$ radical (eqn (10) and (11)).

$$Fe^{3+} + H_2O_2 \rightarrow Fe(OOH)^{2+} + H^+ \quad (7)$$

$$Fe(OOH)^{2+} \rightarrow Fe^{2+} + {}^{\bullet}O_2H \quad (8)$$

$$Fe^{2+} + H_2O_2 \rightarrow Fe^{3+} + OH^- + {}^{\bullet}OH \quad (9)$$

$$Fe^{3+} + {}^{\bullet}O_2H \rightarrow Fe^{2+} + H^+ + O_2 \quad (10)$$

$$Fe^{2+} + {}^{\bullet}OH \rightarrow Fe^{3+} + OH^- \quad (11)$$

Effect of H_2O_2 concentration. The ratio between Fe and H_2O_2 is also an crucial factor that greatly affects electrochemical Fenton process.[31] As observed in Fig. 3c, when the H_2O_2 concentration increased from 10 mM to 30 mM, the RhB degradation using Fenton-like RBCF21, RBCF11, RBCF12 and e-Fenton RBCF12 increased from 66.7, 59.7, 68.3 and 75.3% to 65.3, 80.7, 93.7 and 99.3%, respectively. Since H_2O_2 is the source of $^{\bullet}OH$ generation, as the H_2O_2 concentration increases, more $^{\bullet}OH$ radicals can be generated from the reaction between H_2O_2 and Fe(II).[49] However, as H_2O_2 concentration increased from 20 to 30 nM, the degradation efficiency did not change significantly, as $^{\bullet}OH$ radicals can react with the excess H_2O_2 generate the superoxide radical ($^{\bullet}O_2H$) by-product (eqn (12)), which possesses lower reactivity compared to the $^{\bullet}OH$ radicals owing to their lower oxidizing capacity. Additionally, the excess H_2O_2 cannot be degraded to $^{\bullet}OH$ efficiently due to their limited active sites. As a result, a too high H_2O_2 concentration can negate the RhB degradation. For this reason, in order to minimize the

amount of H_2O_2 but maximize the RhB degradation efficiency, 20 mM H_2O_2 was employed for the next experiment.

$$H_2O_2 + {}^{\bullet}OH \rightarrow {}^{\bullet}O_2H + H_2O \quad (12)$$

Effect of RhB initial concentration. As illustrated in Fig. 3d, higher RhB initial concentration led to lower degradation efficiency. The RhB degradation efficiency was very high at the RhB concentration of 50 mg L^{-1}, being 75.3, 83.0, 94.3 and 95.3% for RBCF21, RBCF11, RBCF12 and e-RBCF12, respectively. When the concentration increased from 50 to 1000 mg L^{-1}, the decomposition efficiency decreased sharply, possibly because increasing RhB can occupy more active sites on the catalyst surface. Therefore, the initial RhB concentration of 100 mg L^{-1} was chosen as a suitable concentration for future investigations.

Effect of electrode distance. In the e-Fenton-based processes, the distance between the electrodes is an important factor as it affects the energy consumption as well as the potential of the system.[50] As observed in Fig. 3e, when the electrode distance varied from 1, 2, 3, and 4 cm, the degradation efficiency first increased from 90% to 99.2%, then decreased slightly from 99.2% to 86.67% and 85.7%, respectively. Generally, reducing the electrode distance can lead to a greater current flow and a lower resistance between the electrodes, as well as shorter passing time of the ions contributing to the e-Fenton process, thus reducing the decomposition efficiency.[51] Furthermore, Fe^{2+} ions that contribute to the process can be regenerated from Fe^{3+} ions due to the effect of electric current on the cathode. There are two factors affecting this process, including the mass transfer of Fe^{3+} across the interface between the solution and the cathode, as well as the electron transfer between Fe^{3+} and the cathode. The longer the distance between the electrodes, the harder the Fe^{3+} mass transfer,[52] thus hindering the catalyst regeneration and reducing the process efficiency. The electrode distance of 1 cm was an exception, with a relatively poor degradation efficiency. This can be explained that very short distance between the electrodes may promote electrode passivation reduce the oxidation capacity of the system, which may consequently hinder the redox process.[53] As a result, an electrode distance of 2 cm is the optimized value to achieve high decomposition efficiency. It can also help bring down the operation costs, as increasing the electrode distance significantly increases energy consumption.[54]

Effect of electric current. In the e-Fenton-based processes, the electric current supplies the necessary energy to facilitate the formation of H_2O_2 and the subsequent generation of $^{\bullet}OH$ (eqn (1) and (3)).[55] As observed in Fig. 3f, as the effect of applied current varied from 50, 100, 150, and 200 mA, the degradation efficiency increased marginally from 76%, 82%, 90%, and 99.3%, respectively. This can be explained that the increased current density can enhance charge distribution over the cathode, resulting in high $^{\bullet}OH$ amount which are very reactive species in the RhB degradation. Increased electric current can also lead to better regeneration of Fe^{2+} ions as mentioned earlier, therefore the degradation efficiency can be further improved. 200 mA yielded the best degradation efficiency; however, upon comparing to that of the electric current of 150 mA, they did not differ significantly (99.3% and 90%, respectively). On the other hand, as the electric current increased, there may be some side reactions that lead to the unnecessary production of peroxyl radicals ($^{\bullet}O_2H$) from $^{\bullet}OH$ radicals (eqn (12) and (13)). In addition, the H_2O_2 reduction on the surface of the cathode (eqn (14)) as well as the reduction of four electrons (eqn (15)) may happen, resulted in the deterioration of the process. Consequently, for high efficiency and low operating cost, the RhB degradation would be conducted at 150 mA.

$$^{\bullet}OH + {}^{\bullet}O_2H \rightarrow H_2O + O_2 \quad (13)$$

$$H_2O_2 + 2H^+ + 2e^- \rightarrow H_2O \quad (14)$$

$$O_2 + 4H^+ + 4e^- \rightarrow 2H_2O \quad (15)$$

The catalyst reusability was investigated over 6 cycles under optimal conditions. After each experiment, the catalyst was filtered and washed several times with distilled water using a vacuum cleaner. As observed in Fig. 4, the degradation efficiency was 91.67% in the first run, 88.67% in the second run, and then dropped gradually to 61.67% by the 6th run, with a loss of about 30% compared to the original degradation efficiency. There are two reasons for this result. First, as RhB is adsorbed on the catalyst surface, it cannot be completely washed away with distilled water. Second, the iron content in the catalyst decreased after each experimental cycle, leading to reduced degradation capability. These results indicate that the catalyst has good stability and reusability for the efficient treatment of RhB and other pollutants.

Fig. 5 presents the amount of sludge generated in the Fenton-like and e-Fenton processes. Compared to the Fenton-like process, the iron sludge formation was reduced in electro-Fenton process. This is because of the continuous Fe^{3+} reduction to Fe^{2+} on the cathode surface (eqn (4)), which could prevent the $Fe(OH)_3$ sludge formation from the dissolved Fe^{3+} ions in the solution.[56,57]

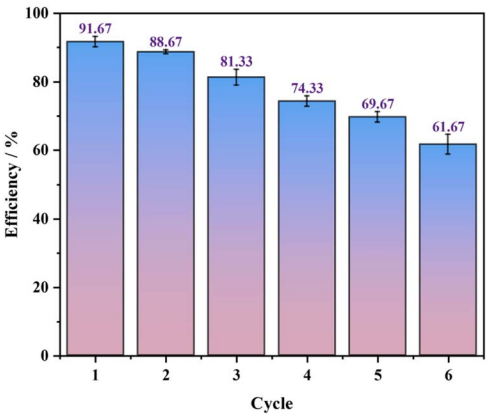

Fig. 4 Recyclability of e-RBCF12 catalyst in the electro-Fenton process for RhB removal efficiency (C_0 = 100 mg L^{-1}, pH = 3, dose = 0.5 g L^{-1}, H_2O_2 = 20 mM, electric current = 150 mA, electrode distance = 2 cm, time = 120 min).

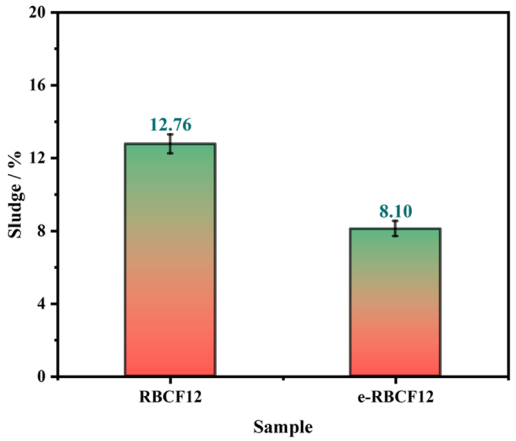

Fig. 5 Sludge formation in the Fenton and electro-Fenton process for RhB removal.

In comparison to some iron-doped catalysts reported in previous studies, the e-Fenton activity of the RBCF12 catalyst exhibited commendable RhB degradation efficiency (Table 3). Although its degradation efficiency was slightly lower, RBCF12 remains a competitive option, particularly considering the cost-effectiveness and the eco-friendliness of using rubber seed shells as a biochar source. Additionally, the magnetic properties of the catalyst, attributed to the incorporation of α-FeOOH, facilitate its easy recovery using an external magnetic field, minimizing material loss during the recycling process, which is a huge advantage compared to the traditional recovery process such as filtration or centrifugation. This highlights the potential of RBCF12 for effective RhB degradation, offering a balance between e-Fenton performance and ecological benefits.

Degradation kinetics

As demonstrated in Table 4, the initial degradation rate constant of RBCF12 is generally higher than that of RBCF21 and RBCF11 at similar operating parameters. This observation indicates that RBCF12 possesses a more rapid and superior degradation capability compared to the other two catalysts. The differences in degradation rates among these samples can be attributed to the amount of iron in their composition, as higher Fe^{3+} content can ameliorate their catalytic activity and degradation efficiency.

Similarly, the initial degradation rate constant of the electro-Fenton process is also superior compared to the Fenton-like process, which signifies that the e-Fenton process is inherently more efficient. The enhanced performance of the e-Fenton process can be attributed to the continuous *in situ* generation of reactive oxygen species, such as hydroxyl radicals, which significantly accelerate the degradation of pollutants.

Moreover, the initial degradation rate increases with the increase of H_2O_2 concentration and the decrease of RhB concentration. Higher concentrations of hydrogen peroxide lead to a greater availability of reactive species, thus enhancing the degradation rate. Conversely, lower pollutant concentrations reduce the competition for reactive sites and allow for more efficient degradation kinetics.

Table 3 Comparison of RhB degradation by Fenton-like and electro-Fenton using different iron-doped biochar catalysts

Catalyst	e-Fenton parameters	Degradation efficiency	Ref.
Fe powder	750 mL of 10 mg per L RhB, pH 3, electrode distance 4 cm, applied voltage 8 V, and contact time 180 minutes	98%	60
Fe-SBA-15	750 mL of 10 mg per L RhB, pH 2, 0.015 g L^{-1} catalyst, electrode distance 3 cm, applied voltage 8 V, and contact time 180 minutes	97.7%	61
Stainless steel (ORR cathode)	5 mg per L RhB, pH 2, 0.5 mM Fe^{2+} catalyst, −5 mA HER current, −400 mV ORR potential, and contact time 120 minutes	97.4%	62
$FeCl_3$ (Bubble column reactor)	50 mg per L RhB, pH 3, 0.005 g L^{-1} catalyst, electrode distance 1.75 cm, applied voltage 3.5 V, and contact time 8 h	98%	63
$MnFe_2O_4$-GO	1000 mL of 10 ppm RhB solution, pH 3, 0.02 g L^{-1} catalyst, electrode distance 1 cm, applied voltage 3 V, and contact time 60 minutes	97.51%	64
RBCF12	500 mL of 100 mg per L RhB solution, pH 3, 20 mM H_2O_2, 0.5 g L^{-1} catalyst, electrode distance 2 cm, electric current 150 mA, and contact time 120 minutes	91.67%	This research

Table 4 Degradation efficiency (at 120 minutes) and Initial degradation rate constant (at 30 minutes) of RhB degradation by Fenton-like and electro-Fenton using RBCF catalysts

Sample	[RhB] (mg L^{-1})	[H_2O_2] (mM)	Degradation efficiency (%) (Fenton-like)	Initial degradation rate constant (mg L^{-1} s^{-1}) × 10^{-5} (Fenton-like)	Degradation efficiency (%) (electro-Fenton)	Initial degradation rate constant (mg L^{-1} s^{-1}) (electro-Fenton)
RBCF21	50	20	74.7	19.8	n/a	n/a
	100	10	65.7	18.4		
	100	15	66.7	15.3		
	100	20	68.0	17.5		
	100	25	67.0	10.7		
	100	30	65.0	13.8		
	150	20	58.3	7.7		
	200	20	52.0	10.1		
	250	20	44.7	9.9		
	500	20	27.3	3.2		
	1000	20	21.3	2.5		
RBCF11	50	20	83.0	47.4	n/a	n/a
	100	10	60.0	13.3		
	100	15	65.0	16.6		
	100	20	73.7	21.4		
	100	25	75.3	29.9		
	100	30	80.7	28.1		
	150	20	62.3	6.3		
	200	20	56.3	11.7		
	250	20	51.0	10.8		
	500	20	31.7	4.3		
	1000	20	26.0	3.6		
RBCF12	50	20	94.3	33.7	95.3	67.8
	100	10	67.7	13.8	75.3	22.3
	100	15	80.0	24.1	81.0	24.5
	100	20	85.7	28.3	90.3	38.1
	100	25	85.0	35.7	96.3	45.1
	100	30	93.0	48.4	99.3	36.5
	150	20	71.7	20.4	77.33	13.0
	200	20	61.3	19.4	63.0	9.8
	250	20	57.3	15.6	57.0	8.8
	500	20	32.7	11.2	40.3	7.3
	1000	20	25.3	10.3	34.7	7.2

Proposed degradation mechanism

The heterogeneous e-Fenton process is a sophisticated oxidation technique that employs solid catalysts to enhance pollutant removal through the fixation of metal ions. This process can be divided into two primary methods: the homogeneous electro-Fenton process, which relies on dissolved metal ions, and the heterogeneous electro-Fenton process, which depends on reactions occurring at the surface of the catalyst.[58,59] In the homogeneous electro-Fenton process, optimal performance is observed at pH values of approximately 3, where the dissolved metal ions are essential for the generation of the reactive radicals. On the other hand, the heterogeneous electro-Fenton process operates efficiently across a wide pH range, as the generation of radicals takes place directly on the surface of the catalyst.

The leaching of iron from the catalysts is a critical aspect of these processes. In the case of goethite, the radical process begins with the formation of a precursor surface complex that incorporates hydrogen peroxide (eqn (16)), followed by a reversible electron transfer reaction that results in the creation of excited state ligands (eqn (17)). The generation of the hydroperoxyl radicals and ferrous ions in this excited state deactivate it and make it unstable (eqn (18)). Subsequent reactions involve either hydrogen peroxide or oxygen interacting with the ferrous ions produced earlier (eqn (19) and (20)). However, the reaction between surface ferrous ions and oxygen is generally slow and can often be disregarded. The decomposition of hydroperoxyl radicals to yield oxygen radicals is a key step in the process (eqn (21)). Additionally, interactions between hydroperoxyl and hydroxyl radicals with surface ferrous and ferric ions (eqn (22) and (23)), as well as hydrogen peroxide, further contribute to the overall reaction dynamics (eqn (24) and (25)). Ultimately, these radical species can terminate their interactions (eqn (26) and (27)), leading to the completion of the reaction cycle. The heterogeneous e-Fenton process is particularly effective under acidic conditions, especially in the context of the first pollutant removal method, as shown in Fig. 6. This understanding of the mechanisms at play in the heterogeneous e-Fenton process highlights its potential for efficient pollutant degradation in various environmental applications.

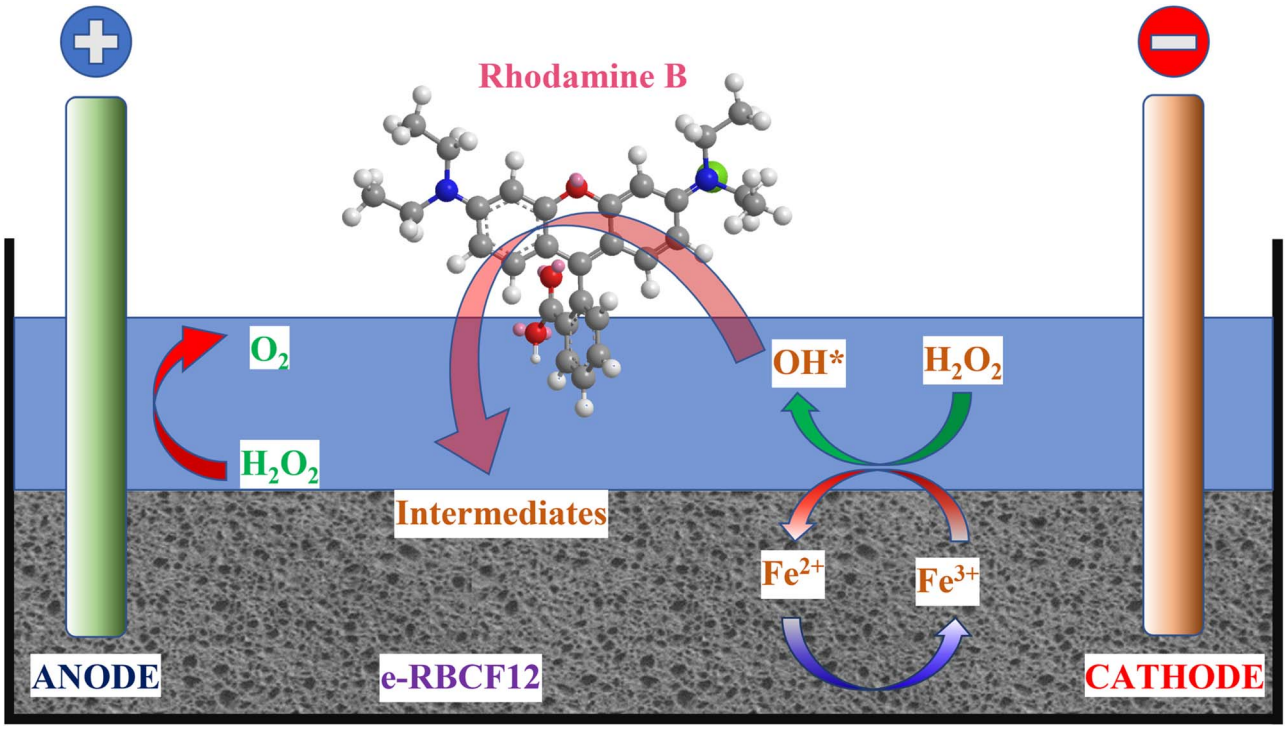

Fig. 6 RhB degradation mechanism of catalyst in electro Fenton process.

$$\equiv Fe^{III}–OH + H_2O_2 \Leftrightarrow (H_2O_2)_S \quad (16)$$

$$(H_2O_2)_S \Leftrightarrow \equiv Fe^{II}O_2{}^{\cdot}H + H_2O \quad (17)$$

$$\equiv Fe^{II}O_2{}^{\cdot}H \Leftrightarrow \equiv Fe^{II} + HO_2{}^{\cdot} \quad (18)$$

$$\equiv Fe^{II} + H_2O_2 \rightarrow \equiv Fe^{III}–OH + H\dot{O} + H_2O \quad (19)$$

$$\equiv Fe^{II} + O_2 \rightarrow \equiv Fe^{III}–OH + HO_2{}^{\cdot} \quad (20)$$

$$HO_2{}^{\cdot} \Leftrightarrow H^+ + O_2{}^{\cdot -} \quad (21)$$

$$\equiv Fe^{III}–OH + HO_2{}^{\cdot}/O_2{}^{\cdot -} \rightarrow \equiv Fe^{II} + H_2O/OH^- + O_2 \quad (22)$$

$$H\dot{O} + \equiv Fe^{II} \rightarrow \equiv Fe^{III}–OH \quad (23)$$

$$H\dot{O} + \equiv Fe^{II} \rightarrow \equiv Fe^{III}–OH + H_2O + HO_2{}^{\cdot} \quad (24)$$

$$(H_2O_2)_S + HO_2{}^{\cdot}/O_2{}^{\cdot -} \rightarrow \equiv Fe^{III}–OH + H\dot{O} + O_2 + H_2O/OH^- \quad (25)$$

$$HO_2{}^{\cdot} + HO_2{}^{\cdot} \rightarrow (H_2O_2)_S + O_2 \quad (26)$$

$$H\dot{O} + HO_2{}^{\cdot}/O_2{}^{\cdot -} \rightarrow H_2O + O_2 \quad (27)$$

Although RBCF12 exhibited good e-Fenton activity, there are still some drawbacks for this process to be applied in practical applications. The Fenton-like process faces challenges such as the requirement for acidic conditions (pH ~ 3), the scalability of catalyst preparation process, including the carbonization of the biomass or biowaste materials together with the incorporation of α-FeOOH, recovery ability and stability of the catalyst, and the complexity of industrial wastewater that may interfere with the e-Fenton process. Future researches will investigate the ability of biochar as a support material and pH stabilizer, or the ability of biochar porous structure in the e-Fenton process coupled with the adsorption process for complicated wastewater system. Different types of biochar will be explored for more sustainable and cost-effective precursors, and long-term stability of the catalysts will be examined to enhance real-world applicability of this process.

Conclusion

In this research, RBCF materials were successfully fabricated from biochar made of rubber seed shell and $Fe(NO_3)_3 \cdot 9H_2O$. The introduction of iron into the RBC materials was verified by XRD, FTIR, SEM, and EDX with good consistency. RBCF12 with 4.78% Fe exhibited high electrochemical Fenton degradation activity, with the maximum removal percentage of approximately 91.67% at the optimized parameters (500 mL solution of 100 mg per L RhB, pH 3, 20 mM H_2O_2, catalyst dose of 0.5 g L^{-1}, electrode distance of 2 cm, electric current of 150 mA, and contact time of 120 minutes). The kinetic studies revealed that the RhB degradation process follows a pseudo-first-order model with the high correlation coefficient under different experimental conditions. Results indicated that the initial degradation rate increased as H_2O_2 concentration increased and RhB concentration decreased. Additionally, the RBCF12 catalyst can be utilized for 6 cycles with negligible loss of catalytic activity, suggesting the potential of iron-doped biochar as the catalyst in

the electrochemical Fenton degradation of RhB and other pollutants in wastewater. Future researches will focus on enhancing different aspects of this e-Fenton catalytic system, making it more plausible for real-world application.

Data availability

The authors declare that the data supporting the findings of this study are available within this published article.

Author contributions

My Linh Nguyen: investigation, writing – original draft and review, funding acquisition, resources, project administration. Thanh Tung Nguyen: investigation, data curation, writing – review and editing. Hoang Long Ngo: methodology, visualization, software, data curation, validation, writing – review.

Conflicts of interest

The authors declare that they have no conflict of interest.

Acknowledgements

It is essential to acknowledge that this work is part of the T2025 project, which received funding from Ho Chi Minh City University of Technology and Education, Vietnam. I would also like to express my sincere thanks for the support from the Faculty of Chemical and Food Technology from HCMC University of Technology and Education, as well to my colleagues for their help in this research.

References

1 V. T. a. A. Association, *Annual Report on Vietnam Textile and Garment Industry*, 2022.
2 V. Research, *Vietnam Textile Industry Overview*, 2022.
3 L. H. Nguyen, H. T. Van, Q. N. Ngo, V. N. Thai, V. H. Hoang and N. T. T. Hai, *Environ. Technol. Innovat.*, 2021, **23**, 101582.
4 E. Commission, *EU Strategy for Sustainable and Circular Textiles*, 2022.
5 UNEP, *Textile Sustainability Reports*, 2021.
6 M. Behera, J. Nayak, S. Banerjee, S. Chakrabortty and S. K. Tripathy, *J. Environ. Chem. Eng.*, 2021, **9**, 105277.
7 H. Guo, Promoting Green Manufacturing in Apparel Companies from a Circular Economy Perspective, Doctoral thesis, Durham University, 2021.
8 D. A. Yaseen and M. Scholz, *Int. J. Environ. Sci. Technol.*, 2018, **16**, 1193–1226.
9 G. Mao, Y. Han, X. Liu, J. Crittenden, N. Huang and U. M. Ahmad, *Chemosphere*, 2022, **288**, 132483.
10 F. Uddin, *Cellulose*, 2021, **28**, 10715–10739.
11 H. T. Van, L. H. Nguyen, T. K. Hoang, T. P. Tran, A. T. Vo, T. T. Pham and X. C. Nguyen, *Sep. Purif. Technol.*, 2019, **224**, 431–442.
12 J. Wu, H. Doan and S. Upreti, *Chem. Eng. J.*, 2008, **142**, 156–160.
13 S. Ranjan Mishra, V. Gadore and M. Ahmaruzzaman, in *Nanohybrid Materials for Water Purification*, Springer, 2022, pp. 97–120.
14 H. Solayman, M. A. Hossen, A. Abd Aziz, N. Y. Yahya, K. H. Leong, L. C. Sim, M. U. Monir and K.-D. Zoh, *J. Environ. Chem. Eng.*, 2023, **11**, 109610.
15 X. Qin, K. Zhao, X. Quan, P. Cao, S. Chen and H. Yu, *J. Hazard. Mater.*, 2021, **416**, 125859.
16 A. S. Ganie, S. Bano, N. Khan, S. Sultana, Z. Rehman, M. M. Rahman, S. Sabir, F. Coulon and M. Z. Khan, *Chemosphere*, 2021, **275**, 130065.
17 G. Repetto and A. del Peso, *Patty's Toxicology*, 2012, pp. 257–354.
18 Y. Zhu, F. Deng, S. Qiu, F. Ma, Y. Zheng and R. Lian, *J. Hazard. Mater.*, 2021, **403**, 123950.
19 C. Sun, T. Chen, Q. Huang, X. Duan, M. Zhan, L. Ji, X. Li, S. Wang and J. Yan, *Sci. Total Environ.*, 2021, **754**, 142136.
20 J. Peng, Z. Wang, S. Wang, J. Liu, Y. Zhang, B. Wang, Z. Gong, M. Wang, H. Dong, J. Shi, H. Liu, G. Yan, G. Liu, S. Gao and Z. Cao, *Chem. Eng. J.*, 2021, **409**, 128176.
21 Z. Luo, M. Liu, D. Tang, Y. Xu, H. Ran, J. He, K. Chen and J. Sun, *Appl. Catal. B Environ.*, 2022, **315**, 121523.
22 G. Gao, Q. Zhang, Z. Hao and C. D. Vecitis, *Environ. Sci. Technol.*, 2015, **49**, 2375–2383.
23 J. Liang, D. Tang, L. Huang, Y. Chen, W. Ren and J. Sun, *Bioresour. Technol.*, 2018, **267**, 524–531.
24 D. Bhatia, N. R. Sharma, J. Singh and R. S. Kanwar, *Crit. Rev. Environ. Sci. Technol.*, 2017, **47**, 1836–1876.
25 A. Kumar, N. K. Srivastava and P. Gera, *J. Environ. Manage.*, 2021, **298**, 113527.
26 M. L. Nguyen, H. L. Ngo, T. T. Nguyen Hoang, D. T. Le, D. D. Nguyen, Q. S. Huynh, T. T. T. Nguyen, T. T. Nguyen and R.-S. Juang, *Iran. J. Environ. Health Sci. Eng.*, 2024, **22**, 313–327.
27 S. S. Sahoo, V. K. Vijay, R. Chandra and H. Kumar, *Clean. Eng. Technol.*, 2021, **3**, 100101.
28 H. Q. Sang, H. N. C. Thong, N. T. Ha, V. T. Y. Linh, N. D. Dat and T. T. K. Anh, *J. Tech. Educ. Sci.*, 2024, **19**, 99–107.
29 M. L. Nguyen, H. L. Ngo, T. T. Nguyen Hoang, D. T. Le, D. D. Nguyen, Q. S. Huynh, T. T. T. Nguyen, T. T. Nguyen and R. S. Juang, *J. Environ. Health Sci. Eng.*, 2024, **22**, 313–327.
30 S. Wang, *Dyes Pigm.*, 2008, **76**, 714–720.
31 S. Xin, G. Liu, X. Ma, J. Gong, B. Ma, Q. Yan, Q. Chen, D. Ma, G. Zhang, M. Gao and Y. Xin, *Appl. Catal. B Environ.*, 2021, **280**, 119386.
32 I. Herath, P. Kumarathilaka, M. I. Al-Wabel, A. Abduljabbar, M. Ahmad, A. R. A. Usman and M. Vithanage, *Microporous Mesoporous Mater.*, 2016, **225**, 280–288.
33 K. Parida and J. Das, *J. Colloid Interface Sci.*, 1996, **178**, 586–593.
34 H. D. Ruan, R. L. Frost, J. T. Kloprogge and L. Duong, *Spectrochim. Acta A Mol. Biomol. Spectrosc.*, 2002, **58**, 967–981.
35 X. Yang, X. Zhang, Y. Ma, Y. Huang, Y. Wang and Y. Chen, *J. Mater. Chem.*, 2009, **19**, 2710–2714.

36 M. Keiluweit, P. S. Nico, M. G. Johnson and M. Kleber, *Environ. Sci. Technol.*, 2010, **44**, 1247–1253.
37 N. K. Gupta, P. Prakash, P. Kalaichelvi and K. N. Sheeba, *Energy Sources, Part A Recovery, Util. Environ. Eff.*, 2016, **38**, 1428–1434.
38 D. Vernekar and D. Jagadeesan, *Catal. Sci. Technol.*, 2015, **5**, 4029–4038.
39 X. Li, K. Cui, Z. Guo, T. Yang, Y. Cao, Y. Xiang, H. Chen and M. Xi, *Chem. Eng. J.*, 2020, **379**, 122324.
40 F. Ghanbari, A. Hassani, S. Wacławek, Z. Wang, G. Matyszczak, K.-Y. A. Lin and M. Dolatabadi, *Sep. Purif. Technol.*, 2021, **266**, 118533.
41 Y. Yi, G. Tu, P. Eric Tsang and Z. Fang, *Chem. Eng. J.*, 2020, **380**, 122518.
42 J. Xu, X. Zhang, C. Sun, J. Wan, H. He, F. Wang, Y. Dai, S. Yang, Y. Lin and X. Zhan, *Environ. Sci. Pollut. Res. Int.*, 2019, **26**, 2820–2834.
43 A. Tiya-Djowe, M. A. Dourges, J. L. Bruneel and H. Deleuze, *RSC Adv.*, 2019, **9**, 4797–4805.
44 M. R. Sohrabi, A. Khavaran, S. Shariati and S. Shariati, *Arab. J. Chem.*, 2017, **10**, S3523–S3531.
45 S. Liu, X.-r. Zhao, H.-y. Sun, R.-p. Li, Y.-f. Fang and Y.-p. Huang, *Chem. Eng. J.*, 2013, **231**, 441–448.
46 W. G. Barb, J. H. Baxendale, P. George and K. R. Hargrave, *Trans. Faraday Soc.*, 1951, **47**, 462–500.
47 M. L. Kremer, *Phys. Chem. Chem. Phys.*, 1999, **1**, 3595–3605.
48 C. Walling and A. Goosen, *J. Am. Chem. Soc.*, 2002, **95**, 2987–2991.
49 M. Nie, Y. Li, J. He, C. Xie, Z. Wu, B. Sun, K. Zhang, L. Kong and J. Liu, *New J. Chem.*, 2020, **44**, 2847–2857.
50 A. Shokri, B. Nasernejad and M. Sanavi Fard, *Water Air Soil Pollut.*, 2023, **234**, 153.
51 S. K. Verma, V. Khandegar and A. K. Saroha, *J. Hazard. Toxic Radioact. Waste*, 2013, **17**, 146–152.
52 S.-H. Thor, L.-N. Ho, S.-A. Ong, C. Z. A. Abidin, C.-Y. Heah, N. Nordin, Y.-P. Ong and K.-L. Yap, *Sep. Purif. Technol.*, 2021, **278**.
53 X. Ren, P. Tang, B. Hou, Z. Yu, J. Huang, Q. Wang and K. Song, *J. Environ. Chem. Eng.*, 2023, **11**.
54 H. R. Zakeri, M. Yousefi, A. A. Mohammadi, M. Baziar, S. A. Mojiri, S. Salehnia and A. Hosseinzadeh, *Int. J. Environ. Sci. Technol.*, 2021, **18**, 3929–3942.
55 N. Barhoumi, N. Oturan, S. Ammar, A. Gadri, M. A. Oturan and E. Brillas, *Environ. Chem. Lett.*, 2017, **15**, 689–693.
56 K. M. Nair, V. Kumaravel and S. C. Pillai, *Chemosphere*, 2021, **269**, 129325.
57 G. Pliego, J. A. Zazo, P. Garcia-Muñoz, M. Munoz, J. A. Casas and J. J. Rodriguez, *Crit. Rev. Environ. Sci. Technol.*, 2015, **45**, 2611–2692.
58 P. V. Nidheesh, H. Olvera-Vargas, N. Oturan and M. A. Oturan, in Electro-Fenton Process, *The Handbook of Environmental Chemistry*, Springer, Singapore, 2017, vol. 61.
59 P. V. Nidheesh, *RSC Adv.*, 2015, **5**, 40552–40577.
60 P. V. Nidheesh and R. Gandhimathi, *Clean: Soil, Air, Water*, 2013, **42**, 779–784.
61 R. Jinisha, R. Gandhimathi, S. T. Ramesh, P. V. Nidheesh and S. Velmathi, *Chemosphere*, 2018, **200**, 446–454.
62 H. Zhang, X. Wan, G. Li and F. Zhang, *Electrochim. Acta*, 2017, **250**, 42–48.
63 P. V. Nidheesh and R. Gandhimathi, *Desalination Water Treat.*, 2015, **55**, 263–271.
64 G. Anil, J. Scaria and P. V. Nidheesh, *Water*, 2022, **14**, 3350.